한국동력기계공학회지 제9권 제2호 pp.5~13 2005년 5월

Experimental and FEM Approach to Develop Optical Engine
가시화엔진 개발을 위한 실험 및 유한요소 해석적 접근

K. S. Lee and M. Y. Baek
이교승 · 백문열

Key Words : Optical Engine(가시화 엔진), Visualization(가시화), FEM(유한요소해석), Stress(응력)

Abstract : 새로운 엔진을 개발하기 위한 중요한 과정 중에 하나로서 엔진 연소실 가시화를 들 수 있다. 그러나 실제 운전상태에 있는 엔진 연소실을 가시화하기 위해서는 극복해야 할 여러 가지 어려운 점들이 있기 때문에, 지금까지는 간단한 실험적 접근방법 혹은 소수의 이론적 해석 방법만이 보고 된 상태이다. 본 연구에서는 가시화용 수정엔진을 개발하기 위해 필요한 몇 가지 중요한 사항들을 다루었다. 즉, 가시화용 수정엔진의 안전한 운전을 위하여 엔진 실린더 외부에 강제대류 효과를 주었고, 또한 실린더 두께 변화에 따른 온도 및 응력장의 분포를 정량적 · 정성적으로 고찰하였으며 다음과 같은 결론을 얻을 수 있었다. 첫째, 실린더 라이너 외벽을 강제대류로 냉각했을 경우, 열응력 감소에 매우 큰 효과를 보았다. 둘째, 가시화용 수정엔진 라이너의 최적 두께를 도출하였다. 셋째, 전통적인 주철 소재의 실린더 라이너와 비교 시, 주철 라이너는 연소에 의한 폭발 압력이 실린더 안전성에 큰 영향을 미치지 않는 것으로 보고 되었으나, 수정 라이너의 경우 연소압력 및 연소에 의한 연소열 모두 중요한 설계 인자임을 입증하였다.

Nomenclature

C_p	specific heat
E	Young's modulus
h	convection heat transfer coefficient
Q_f	heat flux due to friction
Q_{LHV}	low heating value of fuel
Q_w	heat flux to wall
$Q_{w,fire}$	heat flux to wall during firing
$Q_{w,motor}$	heat flux to wall during motoring
β	thermal expansion coefficient
κ	thermal conductivity
ν	poisson's ratio
ρ	density

1. Introduction

Engine cylinder visualization is the most important process to develop the new engine[1]. But this step has a major difficulty that is almost impossible to access the engine on running visually. To visualize inside engine cylinder without any interference, the material of engine cylinder has to be transparent, strong, resistant to thermal stress and able to withstand high temperature. Quartz has been considered seriously as a cylinder material in order to visualize in-cylinder gas motion because of their special material properties.

Quartz is the optical material most commonly used both for commercial purpose and research. The cylinder made of quartz is frequently broken during the engine operation because quartz is very fragile when handled. Quartz is totally different material from conventional engine material, for instance cast-iron or aluminum composite mate rials.

The effort to visualize engine cylinder began with a glass cylinder by Otto in 1872. Withrow and Rassweiler and later Nakanishi et al. were used quartz window mounted L-head engines and photo graphed combustion phenomena[2),3)]. Holtman

접수일 : 2005년 3월 6일
이교승(책임저자) : 경기공업대학 자동차과
E-mail : leeks@kinst.ac.kr Tel. 031-4964-777
백문열 : 경기공업대학 자동차과

and McClure visualized diesel engine flows by a single cylinder with a thick(2.2mm), fused quartz cylinder and operated this engine under motored and limited number of fired cycle condition[4]. A single cylinder research engine made of a 1.72mm thick quartz liner for flow visualization was built by Bates and used for motoring studies[5]. He reported that one of quartz liner survived for 11 months of intermittent operation while accumulating some large chips on the top from mounting errors and some small chips on the bottom from assembly errors. And it finally failed due to thermal stress after a 25minute motoring test.

In previous works reviewed, the optical engine design was a compromise between optical access and engine components. Therefore it is needed to clarify the thermal and mechanical behavior of quartz liner and to identify the best configuration. In order to find the optimum quartz liner configura tion, the steady and transient temperature fields of quartz liner were investigated. And then the steady and the transient stress fields were examined with effects of forced cooling and thickness under the motoring and firing conditions.

2. FEM Analysis

2.1 Modeling and Basic Assumption

A 3-dimensional finite element model(FEM) of the quartz liner was composed and a total of 8,320 nodes and 700 elements were employed to describe the FE model using cartesian coordinate. The baseline liner was modeled as a cylinder recommended by General Motors (height—124.8mm, thickness—13.625mm, outer dia.—119.25mm, inner dia.—92mm). On the inside surface of the cylinder, heat loss from the combustion gas and the heat generation by ring friction were applied. On the outside surface, cooling either by natural or by forced convection was applied. All grids are isoparametric 8-node solid brick. Steady state and transient heat transfer, and stress analyses were accomplished using the commercial codes Hypermesh 3.0(pre- and post- processor) and ABAQUS 5.8 (solver).

In this work, temperature dependent material properties were used and material properties are summarized in Table 1. The heat transfer analysis was conducted first. Subsequently, the heat transfer results and combustion pressure were used to perform the stress analysis.

During the real engine operation, engines are under time varying coupled thermal load (due to heat input from combustion and friction) and mechanical load (due to clamping forces and combustion pressure). To describe realistic engine operating condition by FEM analysis, several reasonable assumptions are needed.

Table 1 Material properties of the quartz liner

Density, ρ, [kg/m^3]	2.2 x 10^3
Young's Modulus, E, [GPa]	70
Poisson's Ratio, ν	0.17
Specific Heat, Cp, [J/kg K]	772 (100℃) 964 (500℃) 1052 (900℃)
Thermal Conductivity, k, [W/m K]	1.36 (20℃) 1.46 (100℃) 1.55 (200℃) 1.67 (300℃) 1.84 (400℃) 2.88 (950℃)
Thermal Expansion Coefficient, β, [1/K × 10^{-7}]	5.1 (100℃) 5.8 (200℃) 5.9 (300℃) 5.4 (600℃) 4.8 (900℃)

In this study, engine operation was assum ed to be quasi-steady state at given time step and cyclic thermal shock effect in thermal penetration depth was ignored. Combustion pressure and heat fluxes were assumed to be constant profiles in time, but varied along the liner longitudinal direction from the liner top. Frictional heat source was assumed to be stepwise function.

Figure 1 shows schematic diagram of imposed boundary condition.

2.2 Boundary conditions

The cylinder was modeled with specified top and bottom temperatures. And in order to impose thermal and mechanical boundary conditions, FEM model was divided by several regions (see Fig. 1) and details are shown in Table 2. A1-A6 and F1-F22 indicate areas where boundary conditions were imposed and %s indicate applied heat fluxes from combustion(Q_w) and friction(Q_f).

(a) Heat flux from combustion gas to the liner, Q_w

In this case, it was assumed to be 10 % of $\dot{m}_f Q_{LHV}$ because there is no heat loss to cylinder head for firing condition suggested by General Motors and based on experiment[6].

$$\dot{m}_f = 1.13 \text{ kg/h}$$
$$Q_{w,fire} = 511{,}523 \text{ W/m}^2$$

For motoring, the total heat transfer loss from the gas is equal to the integral of PdV during a cycle. The amount of heat going into the liner was assumed to be 1/3 of the total value suggested by General Motors and based on experiment[6].

$$Q_{w,motor} = 7{,}444 \text{ W/m}^2$$

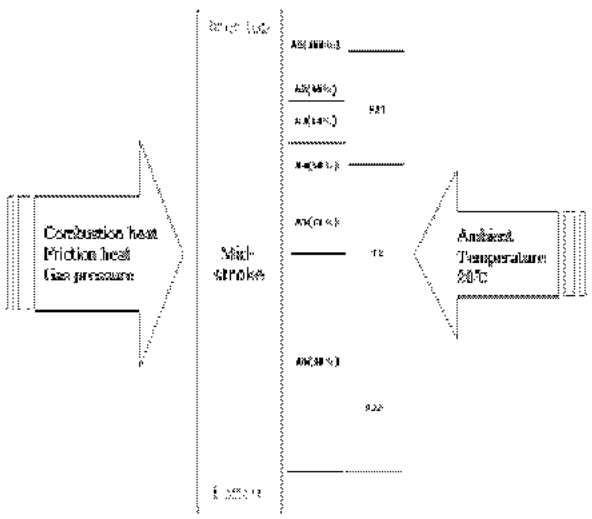

Fig. 1 Schematic diagram of the quartz liner for boundary conditions

Table 2 Thermal and mechanical boundary conditions

		Motoring / Applied	Firing / Applied
Heat flux from gas to wall, Q_w, [W/m^2]	A1	7444 / 3722	51152 / 25576
	A2	6700 / 3350	46037 / 23018
	A3	4764 / 2382	32737 / 16368
	A4	3722 / 1861	25576 / 12788
	A5	2605 / 1861	17903 / 8951
	A6	2233 / 1116	15345 / 7673
Friction heat input Q_f, [W/m^2]	F1	/ 4617	/ 6925
	F21,F22	/ 2309	/ 3463
Convective heat transfer coeffi., h, [W/mK]	Natural	8	10
	Forced	39	52
		Motoring	Firing
In-Cyl. gas pressure, P, [kPa]	A1	2000	6000
	A2	1800	5000
	A3	1500	3500
	A4	1000	2000
	A5	500	800

(b) Heat flux to liner due to friction, Q_f

Heat transfer come from friction is basically 1.5 % of $\dot{m}_f Q_{LHV}$ for firing condition suggested by General Motors and based on experiment[6].

$$Q_{f,fire} = 6{,}925 \text{ W/m}^2$$

And also it was assumed to be about 70 % based on experimental data for motoring condition of the firing condition value.

$$Q_{f,motor} = 4{,}640 \text{ W/m}^2$$

(c) Heat transfer coefficient for natural convection, h_n

Vertical flat plate correlation was used for the fired and motored operation[7].

(d) Heat transfer coefficient for forced convection, h_f

Equation around the cylinder shaped object was used for both of the fired and motored operation[7]. It was assumed that nozzle tip

velocity was 5m/s and nozzle diameter was assumed to be 0.1m.

(f) Coolant temperature

The coolant temperature in head and bottom were assumed to 90℃ and 30℃, respectively.

(g) In-cylinder gas pressure in kPa

During the motoring, it was assumed as if hydrostatic pressure distribution along the longitu dinal direction of the liner based on experimental data. While there are no firing data, it was also assumed based on similar engine operating conditions.

(h) Mechanical constraints

As mechanical constraints for the stress analysis, some nodes located in top and bottom were fixed ($x = y = z = 0$).

(i) Engine operating condition

Engine speed was 1200rpm and full load condi tion.

3. Validation of FEM Model

In order to validate the FEM model, transient temperature at the selected points of the thermal field was compared with measurements recorded at the same points.

Table 3 Specification of test engine

Bore	Stroke	Con. rod	Liner length	Liner thickness	Comp. ratio
92mm	96mm	223.5mm	124.8mm	13.625mm	9.5

3.1 Engine set-up

A single quartz cylinder was used for this experiment and the engine specification is shown in Table 3. Three thermocouples were located at outside quartz cylinder. The high means 5mm away, mid means 55mm away, and low means 82mm away from the liner top, respectively. The temperature was recorded under the following conditions; motored at 1200rpm, 30℃ intake air temperature and 90℃ cylinder head coolant tem perature, 100kPa manifold pressure, and uncharac terized air-jet as external forced cooling. Here the number of air jet nozzle was 4 and those nozzles were located 200mm away from outside cylinder with 90°, respectively.

3.2 Temperature field comparison

Measured and predicted surface temperatures at given locations, 5(high), 55(mid), and 82(low)mm away from the liner top, were compared in Figures 2 and 3, where E- and C- indicate experiment and computational data, respectively. In general, predicted data are larger than those of experiment. Under the natural convection condition, the highest temperature achieved from experiment is recorded at the mid-point, followed by low and high as well as computation data. But some differences in magnitude are observed.

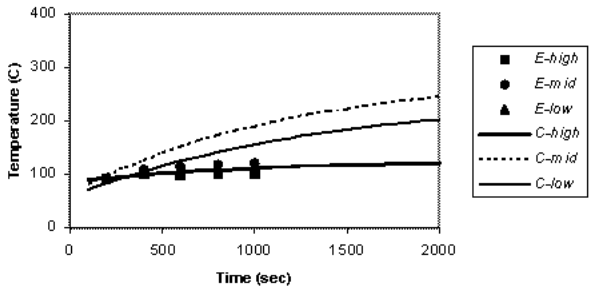

Fig. 2 Comparison between measured and predicted transient outside surface temperature of quartz liner under natural convection condition. (E:experiment, C:computation)

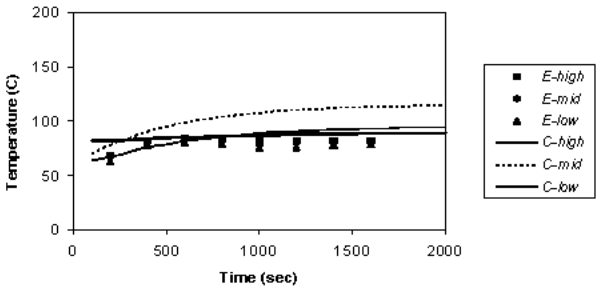

Fig. 3 Comparison between measured and predicted transient outside surface temperature of quartz liner under forced convection condition. (E:experiment, C:computation)

Under the cooled condition, the highest tempera ture achieved from experiment is recorded at the high-point, followed by low and mid. On the other hand, the order of magnitude of computation data is mid, low and high-points. Though there are some differences in order of magnitude, each value is satisfactory.

The discrepancies above can be attributed to the following reasons. First, there is possibility of maldistribution of cooling air-jet under cooled condition. In general under the motoring condition, main heat source is friction. Hence, the tempera ture of mid-stroke is expected higher than that of other location. Second, there are lots of assump tions to impose thermal boundary conditions because of lack of basic experimental data about thermal behavior phenomena in optical engine. However, the FEM model presented in this study has the potential to capture the thermal and stress fields within the quartz liner with acceptable accuracy even with simple approach.

4. Stress Distribution

4.1 Effect of forced cooling

The effects of natural convection and intensive forced convection were examined in order to validate effectiveness of forced cooling. FEM predictions of transient thermal stress distribution in the quartz liner are shown in Figures 4 to 7 for several time step and the results are summarized in Table 4. The (a), and (b) indicate the case of natural and forced cooling, respectively.

Table 4 Summary of forced convection effect, maximum thermal stress[MPa]

	1 sec	10 sec	100 sec	900 sec	2200 sec	Steady state
Natural convection	25.3	25.5	29.5	54.4	64.8	67.1
Forced convection	25.3	25.3	28.2	41.7	43.7	43.8

Through Figures 4 to 7, while the general characteristic of iso-stress distribution was similar, the magnitude of stress and deformation increased gradually as time is increasing.

Higher stress concentration region was observed on the outside surface of the top and bottom. And maximum thermal stress was observed in that region. Inside surface of the quartz liner has also slightly higher level of thermal stress.

At the early stage of combustion (before 100 second), the magnitude and the maximum thermal stress level were similar in each cases.

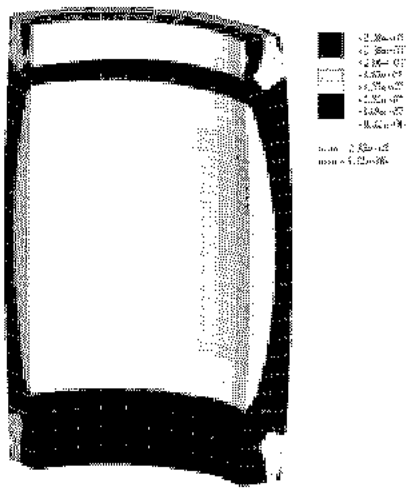

(a)

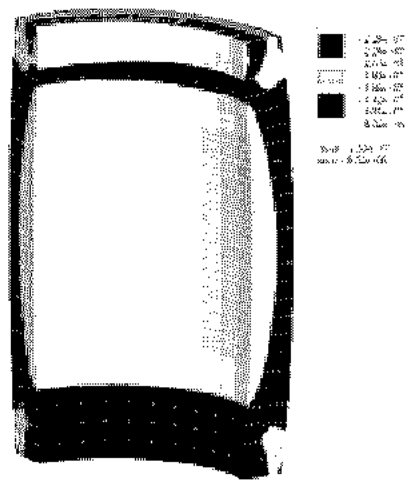

(b)

Fig. 4 Transient thermal stress[MPa] distribution of the quartz liner with deformation at 10 second after firing
(a) natural convection (b) forced convection

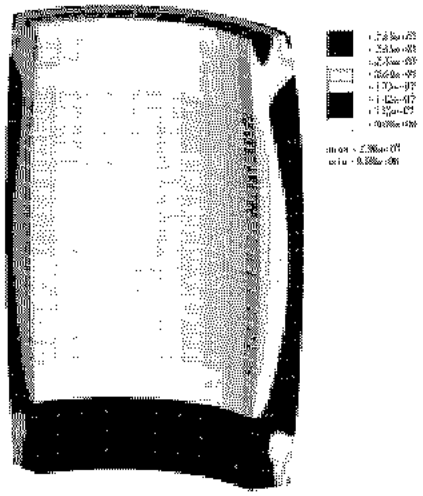

(a)

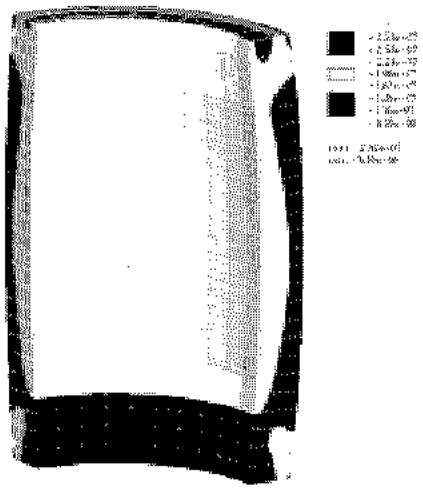

(b)

Fig. 5 Transient thermal stress[MPa] distribution of the quartz liner with deformation at 100 second after firing
(a) natural convection (b) forced convection

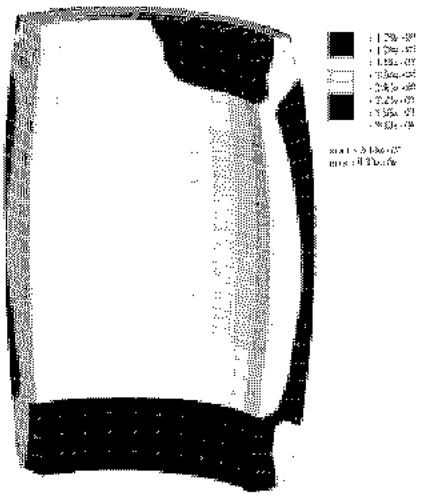

(a)

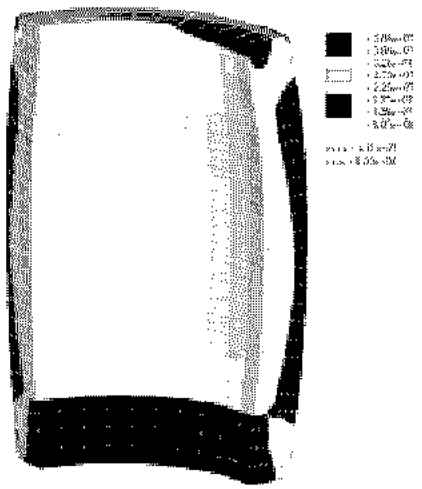

(b)

Fig. 6 Transient thermal stress[MPa] distribution of the quartz liner with deformation at 900 second after firing
(a) natural convection (b) forced convection

But as time passed, the difference between each case increased gradually and then at steady-state the maximum thermal stress of natural convection case is 153% of that of forced convection. Therefore, forced cooling of the outside quartz liner is very helpful to decrease the maximum thermal stress level.

4.2 Effect of liner thickness

The liner thickness was changed based on that of baseline engine to investigate the effect on stress distribution.

As shown in Table 5, for stress due to thermal, the thinner the thickness of the quartz liner was, the smaller the stress level became, because temperature distribution became more uniform. Hence thermal stress decreased gradually.

For stress due to combustion pressure, the thicker the thickness of the quartz liner was, the smaller the stress level became. Because of the effect of reinforcement, the safety factor was increased.

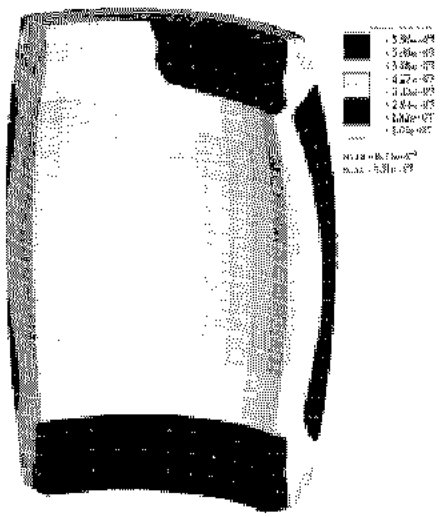

(a)

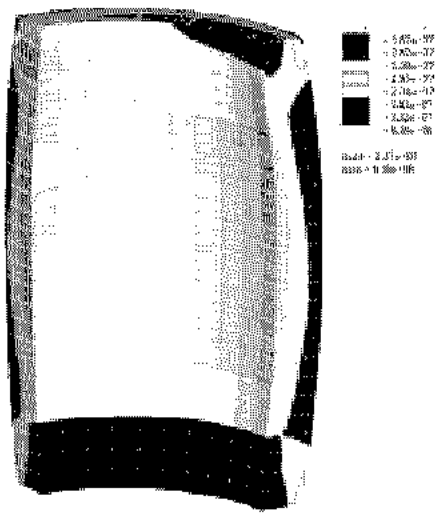

(b)

Fig. 7 Steady-state thermal stress[MPa] distribution of the quartz liner with deformation
(a) natural convection (b) forced convection

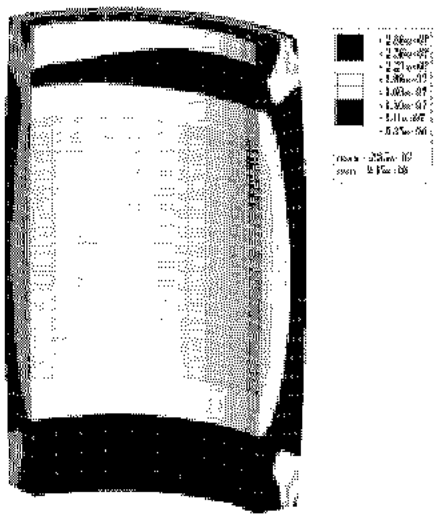

(a)

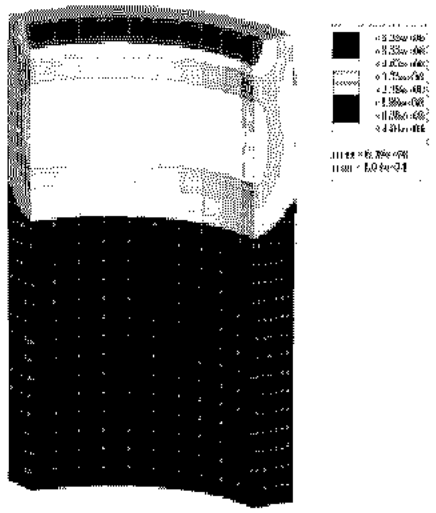

(b)

Fig. 8 Steady-state stress[MPa] distribution of quartz liner during motoring
(a) due to thermal (b) due to mechanical

Table 5 Summary of liner thickness effect, steady-state stress[MPa]

Model thickness [mm]	Stress due to thermal	Stress due to combustion pressure	Combined stress
10	42.2	23.0	58.6
11.5	43.0	20.2	56.6
13.625	43.8	17.4	54.6
15.5	44.3	15.5	53.4
17.0	44.5	14.4	52.2

For stress due to both thermal and combustion pressure, the thicker the thickness of the quartz liner was, the smaller the stress level became gradually, because the decreasing rate of stress due to thermal was smaller than that of mechanical stress caused from combustion press ure.

4.3 Effect of thermal and mechanical loading

In order to investigate the relative import ance between thermal and mechanical loading, the results was shown in Figures 8 and 9. Figures

8 and 9 are shown the predicted stress distribution of the quartz liner during motoring and firing operation, respectively. In general, for the cast-iron, it has been known that the effect of mechanical loading will be negligible. For the quartz liner, however, stress due to combustion pressure is not negligible any more because the relative magnitude of mechanical stress due to combustion pressure was 37.9 % of that of thermal stress. Hence for the quartz liner, mechanical stress should be con sidered deliberately.

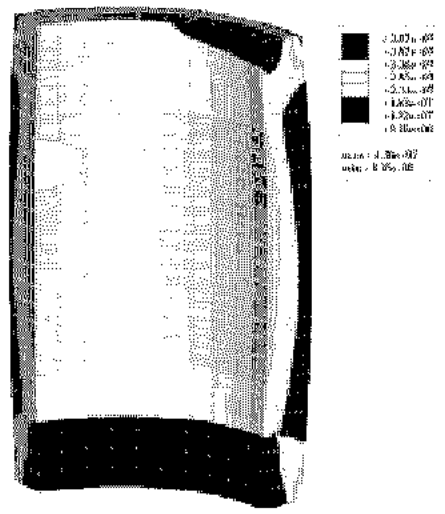

(a)

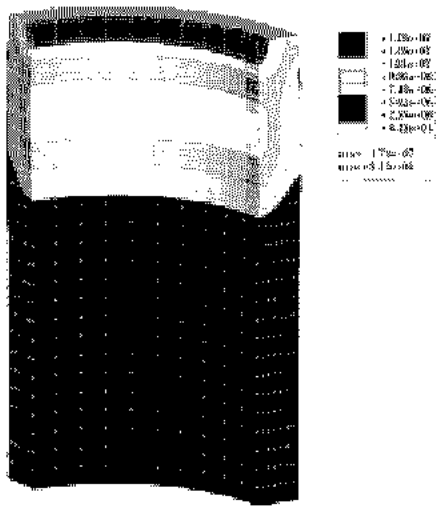

(b)

Fig. 9 Steady-state stress[MPa] distribution of quartz liner during firing
(a) due to thermal (b) due to mechanical

5. Conclusion

Simple FEM model was presented and simulation data were compared with experimental data to operate visual quartz engine safely under firing condition. And it has given us several qualitative and quantitative results of temperature and stress fields in the quartz cylinder. The following conclusions drawn from this study can be useful for improving current quartz engine technique.

1. Forced convection of outside quartz liner is very helpful to decrease the thermal stress level.
2. To find the optimal thickness of the quartz liner is basic design problem and it should be determined with considering of strength, price and other reasons. Under given condition in this study, 13.625mm was found optimum thickness.
3. For conventional engine materials, mechanical load due to combustion pressure is known to be negligible. However for the quartz liner, the relative magnitude of mechanical stress takes a large portion of total stress. Hence, the mechani cal stress should be considered deliberately such as reinforcement.

References

1. M. Namazian, S. Hansen, E. Lyford-Pike, J. B. Heywood and J. Rife, 1980, "Schlieren Visualization of the Flow and Density Fields in the Cylinder of a Spark-Ignition Engines", SAE 800044, pp. 1-18.
2. L. Withrow and G. M. Rassweiler, 1936, "Slow-Motion Shows Knocking and Non-Knocking Explosion", SAE Transaction, 39, pp. 297-303.
3. K. Nakanishi, T. Hirano, T. Inoue and S. Ohigashi, 1975, "The Effect of Charge Dilution on Combustion and Its Improvement Flame Photograph Study", SAE 750054.

4. R. L. Holtman and P. B. McClure, 1978, Detroit Diesel Allison, Indianapolis, Indiana, Private Communication.
5. S. C. Bates, 1988, "A Transparent Engines for Flow and Combustion Visualization Studies", SAE 880520, pp. 1-13.
6. General Motors, 2000, Deer Born Lab., MI, U.S.A., Private Communication.
7. F. P. Incropera and J. W. Dewitt, 1985, "Introduction to Heat Transfer", 2nd Edition, John Wiley & Sons, New York, pp. 301~430.